# Directed motion of metallodielectric particles by contact charge electrophoresis

Yong Dou,<sup>†</sup> Charles A. Cartier,<sup>‡</sup> Wenjie Fei,<sup>†</sup> Shashank Pandey,<sup>†</sup> Sepideh Razavi,<sup>¶</sup> Ilona Kretzschmar,<sup>¶</sup> and Kyle J. M. Bishop<sup>\*,†</sup>

†Department of Chemical Engineering,

Columbia University, New York, NY, 10027

‡Department of Chemical Engineering,

The Pennsylvania State University, University Park, PA 16802

¶Department of Chemical Engineering,

City College of the City University of New York, New York, NY 10031

E-mail: kyle.bishop@columbia.edu

#### Abstract

We investigate the dynamics of metallodielectric Janus particles moving via contact charge electrophoresis (CCEP) between two parallel electrodes. CCEP uses a constant voltage to repeatedly charge and actuate conductive particles within a dielectric fluid resulting in rapid oscillatory motion between the electrodes. In addition to particle oscillations, we find that micron-scale Janus particles move perpendicular to the field at high speeds (up to 600  $\mu$ m/s) and over large distances. We characterize particle motions and propose a mechanism based on the rotation-induced translation of the particle following charge transfer at the electrode surface. The propulsion mechanism is supported both by experiments on fluorescent particles that reveal their rotational motions and by simulations of CCEP dynamics that capture the relevant electrostatics

and hydrodynamics. We also show that interactions among multiple particles can lead to repulsion, attraction, and/or cooperative motions depending on the position and phase of the respective particle oscillators. Our results demonstrate how particle asymmetries can be used to direct the motions of active colloids powered by CCEP.

## Introduction

Active colloidal particles harness energy from their environment to power directed motions relative to their fluid surroundings. <sup>1-3</sup> Inspired by the locomotion of micro-organisms, <sup>4</sup> these artificial swimmers are actively pursued for their potential to navigate complex environments <sup>5,6</sup> and deliver cargo to targeted locations. <sup>7,8</sup> Fluid flows induced by particle motions can also serve to enhance rates of mass transfer to/from the particle surface with emerging applications in water remediation <sup>9,10</sup> and chemical detection. <sup>11,12</sup> When many active particles get together, they often interact to form dynamic assemblies <sup>13</sup> such as swarms, <sup>14,15</sup> flocks, <sup>16</sup> clusters, <sup>17</sup> and crystals. <sup>18</sup> Synthetic realizations of such active matter <sup>19</sup> provide useful models by which to explore the many forms of self-organization that arise outside of thermodynamic equilibrium. Importantly, the diverse behaviors of active particles depend critically on the specific mechanism of propulsion and on the associated interactions among the particles. Expanding the repertoire of active colloids can therefore enable the discovery of new dynamical behaviors as well as the development of future applications.

A wide variety of physicochemical mechanisms have been applied to power the motion of active colloids. Self-phoretic mechanisms<sup>20</sup> use asymmetries in particle shape and/or composition to create local gradients in the electric potential,<sup>21</sup> chemical composition,<sup>22</sup> or temperature<sup>23</sup> that drive particle motions via interfacial phoretic effects such as electrophoresis, diffusiophoresis, or thermophoresis, respectively.<sup>24</sup> In a classic example,<sup>25,26</sup> bimetallic nanorods move autonomously through a homogeneous liquid containing a suitable chemical fuel via reaction-induced self-electrophoresis.<sup>27,28</sup> The motion of asymmetric particles can also be powered by external fields. Alternating electric fields drive motions of polarizable

particles by induced charge electrophoresis; <sup>29–31</sup> alternating magnetic fields power the swimming of flexible magnetic particles by inducing non-reciprocal beating motions; <sup>32</sup> acoustic fields propel dense metallic particles by directing steady streaming flows. <sup>33–35</sup> Characteristic of colloidal swimmers, these types of field-driven motion allow particles to move freely in multiple directions (typically those perpendicular to the applied field). The use of external fields to power such motions is attractive for studies of active matter as their magnitude can be varied in space and time.

Here, we describe a type of colloidal propulsion in which an electric field drives the autonomous motion of metallodielectric Janus particles <sup>36,37</sup> within an insulating liquid between two parallel plane electrodes (Fig. 1a). Similar configurations have been used to investigate particle motions powered by induced charge electrophoresis within conductive liquids $^{31}$  and by Quicke rotation within weakly conductive liquids. 16 By contrast, field-driven motion of conductive particles in insulating liquids is driven by contact charge electrophoresis (CCEP) whereby particles acquire charge on contact with a biased electrode and then move in the field emanating from that electrode. 38-40 In one well studied example, a conductive sphere immersed in mineral oil oscillates rapidly between two electrodes subject to a constant voltage. 40 Each time the particle contacts an electrode, it acquires charge of opposite polarity and moves back towards the other electrode thereby transporting charge down the applied potential gradient. Harnessing these motions for useful functions requires strategies by which to rectify particle oscillations. One approach is to modify the electrodes with asymmetric, ratchet-like features that enable directed transport of conductive particles <sup>38</sup> or droplets. <sup>41</sup> Here, we introduce an alternative strategy that relies on particle asymmetries to achieve similar directed motions.

We show that oscillations of Janus particles between two parallel electrodes are accompanied by steady motions directed perpendicular to the applied field. Through experiment and theory, we develop and validate a mechanism of self-propulsion whereby the field-induced rotation of the particle upon charge reversal at the electrode surface results in its net dis-

placement during each oscillation cycle. Repeated displacements in a common direction propel Janus particles at speeds of up to 600  $\mu$ m/s along wide circular arcs within the plane of the electrodes. Beyond the dynamics of individual particles, we show how particles can both attract or repel one another depending on their separation and on the phases of their respective oscillations. Together, these results demonstrate how particle symmetry can be used to direct the motions of active colloids powered by CCEP. The ability to engineer the motions of individual particles and their assemblies will ultimately contribute to the realization of colloidal machines that organize and operate autonomously to perform useful functions. <sup>42</sup>

# **Experimental Section**

In a typical experiment, a dilute suspension of Janus particles in mineral oil was sandwiched between two parallel electrodes separated by a distance  $H=50-250~\mu m$  (Fig. 1a). We used two types of Janus particles: 8  $\mu m$  silica particles and 4  $\mu m$  fluorescent polystyrene particles, each coated on one hemisphere by a thin layer of gold. In the absence of an applied field, the particles settled to the surface of the lower electrode where they were imaged from above by an optical microscope. Application of a constant voltage  $V=200-1000~\rm V$  caused the particles to oscillate rapidly between the electrodes, as evidenced by their periodic appearance and disappearance from the focal plane (Fig. 1b). Each time a particle came into focus, its position was displaced slightly from that in the previous cycle. The magnitude and direction of these displacements was relatively constant from one cycle to the next resulting in steady particle motions perpendicular to the applied field. Using high speed imaging, we quantified the frequency f of particle oscillations as well as the particle position ( $x_p, y_p$ ) at each oscillation cycle. For example, at  $V=400~\rm V$  and  $H=200~\mu m$ , a silica Janus particle oscillated between the electrodes at an average frequency of  $f=29~\rm Hz$  and moved perpendicular to the field at an average speed of  $U_{\perp}=25~\mu m/s$  (Fig. 1c). Directed particle

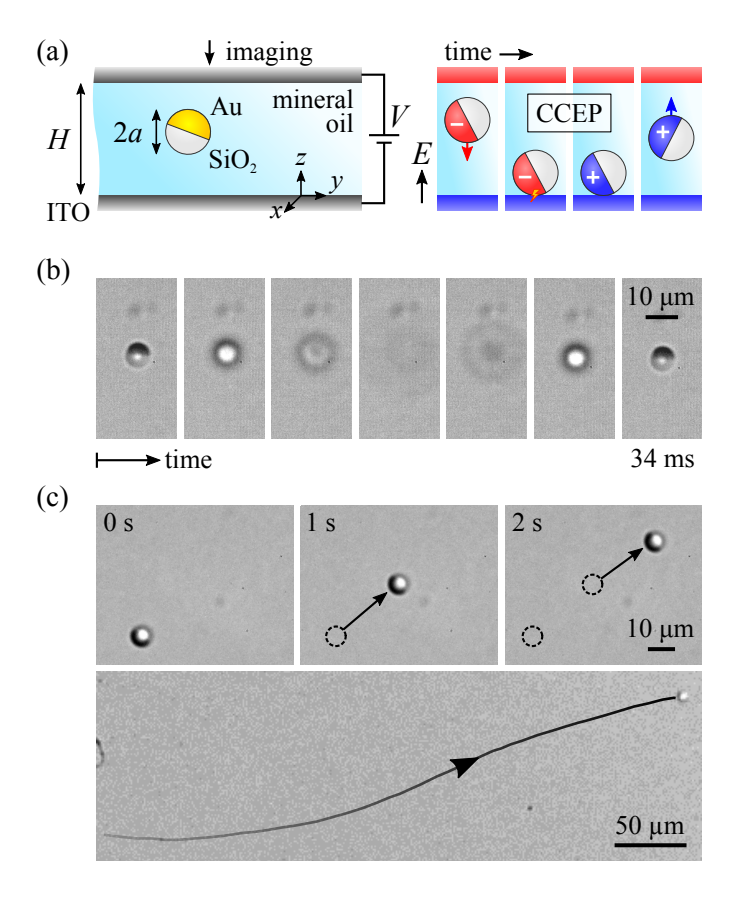


Figure 1: (a) Schematic illustration of the experimental setup. A metallodieletric Janus particle is immersed in mineral oil between two parallel ITO electrodes (left). Application of a constant voltage V results in the oscillatory motion of the particle via contact charge electrophoresis (CCEP; right). (b) When imaged from above, the particle moves in and out of focus in time as it oscillates between the electrodes. (c) Over many oscillation cycles, the particle moves steadily away from its conductive hemisphere (top); the steady motion of the particle continues over hundreds of microns (bottom). See supporting videos 1, 2, and 3.

motion continued over large distances for as long as the voltage was applied. Reversing the sign of the applied voltage did not alter the direction or speed of particle motions.

#### Synthesis of Janus Particles

Silica Janus particles were prepared by deposition of gold onto particle monolayers supported on glass slides. Following Prevo and Velev,  $^{43}$  10  $\mu$ L of a concentrated (30 wt%) suspension of 8  $\mu$ m silica particles in water was placed between two acid-cleaned microscope slides mounted at an angle on a motorized stage (Harvard Apparatus PHD 2000). The trapped colloidal solution was dragged at a prescribed speed by the motion of the top slide to achieve well-packed monolayers. Successive layers of metal (5 nm Ti and 10 nm Au) were then deposited by physical vapor deposition (Cressington 308).

Fluorescent Janus particles were prepared following a procedure adapted from Kopelman et al. <sup>44</sup> Briefly, sulfonated fluorescent polystyrene particles (ThermoFisher F8858) were washed three times in water by centrifugation and dispersed in methanol at a concentration of 1% w/v. 0.5 ml of the particle suspension was deposited onto a 4-inch silicon wafer by spin coating at 2500 rpm for 15 sec. Successive layers of metal (5 nm Ti, 25 nm Ni, and 20 nm Au) were then deposited by e-beam evaporation (Kurt J Lesker Co. Lab 18). The nickel layer was included for a purpose unrelated to the present experiments and is unnecessary here. The particles were gently brushed off the wafer using a damp brush.

## **Electrode Configuration**

The electrode setup was comprised of two transparent indium tin oxide (ITO)-coated glass slides (SIGMA-Aldrich, CAS:50926-11-9, surface resistivity 70-100  $\Omega/\text{sq}$ ) separated from one another by spacers made of glass (150  $\mu$ m to 250  $\mu$ m thick cover slides) or polydimethylsiloxane (PDMS, 50  $\mu$ m to 100  $\mu$ m thick). The ITO electrodes were connected to a high-voltage source (Keithley 2410) with a limiting current of 10  $\mu$ A to prevent damage to the system in the event of a short-circuit. The Janus particles were dispersed in Nylon membrane-

filtered mineral oil (SIGMA-Aldrich, CAS:8042-47) at a concentration of 0.01 - 1 mg/ml and injected into the inter-electrode region. The charge relaxation time for mineral oil was  $\varepsilon/k \sim 20$  s, where  $\varepsilon$  is the permittivity, and k is the electrical conductivity. <sup>39</sup> As this time scale was much larger than the particle oscillation period (ca. 0.01 s), the finite conductivity of the fluid could be safely neglected. <sup>39</sup> The field-induced motion of the Janus particles was captured by a high speed camera (Phantom V310) mounted on an optical microscope (Zeiss Axio Imager A1) operating in bright field mode with 10x and 50x objectives.

#### Particle Tracking

Movies were captured at frame rates of 1,000 – 5,000 fps and processed in MATLAB to analyze particle oscillations and reconstruct particle trajectories. To determine the oscillation frequency, we first identified a fixed window around a single particle and computed the window-averaged pixel intensity for each frame. This average intensity oscillated in time as the particle moved into and out of focus, reaching its local minimal value when the particle came into focus at the lower electrode. For each oscillation cycle i = 1, 2, ..., N, we identified the time  $t_i$  when the particle contacted the lower electrode. The mean oscillation frequency was then computed by dividing the number of particle oscillations by the total observation time,  $f = N/(\Sigma_i t_i)$ . To reconstruct particle trajectories  $(x_i, y_i)$ , we considered only those frames when the particle was in focus (i.e., when the average intensity was in local minimum) and determined the location of the particle center using standard algorithms. The net displacement for cycle i was computed as  $\Delta_i^2 = (x_{i+1} - x_i)^2 + (y_{i+1} - y_i)^2$ ; the average speed of the particle (parallel to the electrodes) was computed as  $U_{\perp} = (\Sigma_i \Delta_i)/(\Sigma_i t_i)$ .

#### Simulation of CCEP Motions

The model of CCEP dynamics combines classical electrostatics and low Reynolds number hydrodynamics.<sup>40</sup> The metallic hemisphere of the Janus particle as well as the bounding electrodes were treated as perfect conductors. To facilitate our numerical analysis, the con-

ductive portion of the particle was modeled as a solid hemisphere with rounded corners (radius 0.1a) in contrast to the thin hemispherical cap present in experiment. Additionally, the non-metallic hemisphere and the surrounding fluid were assumed to be dielectrics with a common permittivity  $\varepsilon$ . Given the particle charge q, orientation  $\alpha$ , and height  $z_p$  above the electrode surface, we solved the Laplace equation numerically to determine the electric potential  $\Phi$  and field  $\mathbf{E} = -\nabla \Phi$  throughout the dielectric medium (see Supporting Information for details). We then integrated the Maxwell stress over the surface of the conductive hemisphere to determine the electric force and torque that drive particle motion.

At low Reynolds numbers (in experiments  $Re \leq 0.01$ ), the translational and rotational velocities of the particle are linearly related to the external force and torque by the so-called resistance tensor.  $^{46,47}$  For a spherical particle near a solid plane boundary, there exist exact analytical expressions  $^{46}$  for the components of this tensor, which, when suitably rescaled, depend only on the separation between the sphere and the plane. Using these expressions, we computed the particle velocity and integrated numerically to determine the position and orientation of the particle as a function of time. We assumed that the charge q on the particle remained constant until the surface of the metallic hemisphere reaches some critical separation  $\delta$  from the plane electrode, at which point charge flowed to/from the particle instantaneously to reverse the particle polarity  $(q \to -q)$ . Physically, the contact charging process is thought to occur by an electric discharge; the resulting charge on the particle is somewhat variable but consistently less than that expected at equilibrium (i.e., when the potential on the particle equals that of the electrode). After nondimensionalization, the computed particle trajectories depend on just two parameters: the dimensionless charge  $q/4\pi\varepsilon a^2E$  and the dimensionless separation at contact  $\delta/a$ .

#### Results and Discussion

Figure 2a shows the reconstructed trajectories of six different Janus particles under identical conditions over the course of one hundred oscillation cycles based on the experiment results. The cumulative displacement of each particle increased roughly linearly with the number of oscillations (Fig. 2b) as the particles moved along wide circular arcs of radius 20  $\mu$ m or greater. These observations are consistent with the spatial homogeneity of the applied field, which suggests that particle motion be invariant to translation and rotation in the xy plane of the electrodes. Although the majority of particles (ca. 70% for V=800 V and H=200  $\mu$ m) exhibited such directed motions, some Janus particles were observed to oscillate between the electrodes with no lateral motion whatsoever. Additionally, some particles (ca. 20%) remained "stuck" to the electrode surface and did not move at all upon application of the field.

For the particles that moved, the oscillation frequency increased monotonically with increasing voltage as  $f \propto V^2$  (Fig. 2c). This observation is consistent with previous studies of CCEP motion, which showed that the oscillation frequency scales as  $f \sim \varepsilon a V^2/\eta H^3$ , where  $\eta$  is the fluid viscosity, and a is the particle radius. <sup>40</sup> By contrast, the lateral displacement of the particle during each oscillation cycle was largely independent of the applied voltage; each oscillation contributed an average displacement of  $\Delta = 0.2a$  (Fig. 2d). Consequently, the lateral velocity of the particle,  $U_{\perp} \equiv f\Delta$ , also increased as the square of the applied voltage (Fig. 2e). This velocity could be further increased by decreasing the spacing between the electrodes H to increase the magnitude of the applied field (Fig. 2f). Using spacers of  $H = 50 \ \mu\text{m}$ , we observed particles velocities up to  $U_{\perp} = 600 \ \mu\text{m}/\text{s}$  in the direction perpendicular to the applied field.

To explain these experimental observations, we propose the following propulsion mechanism illustrated in Figure 3a. As it moves across the channel, a charged Janus particle adopts a preferred orientation in which its principal axis is oblique to the applied field and its motion is directed towards the metallic hemisphere. When it contacts either electrode,

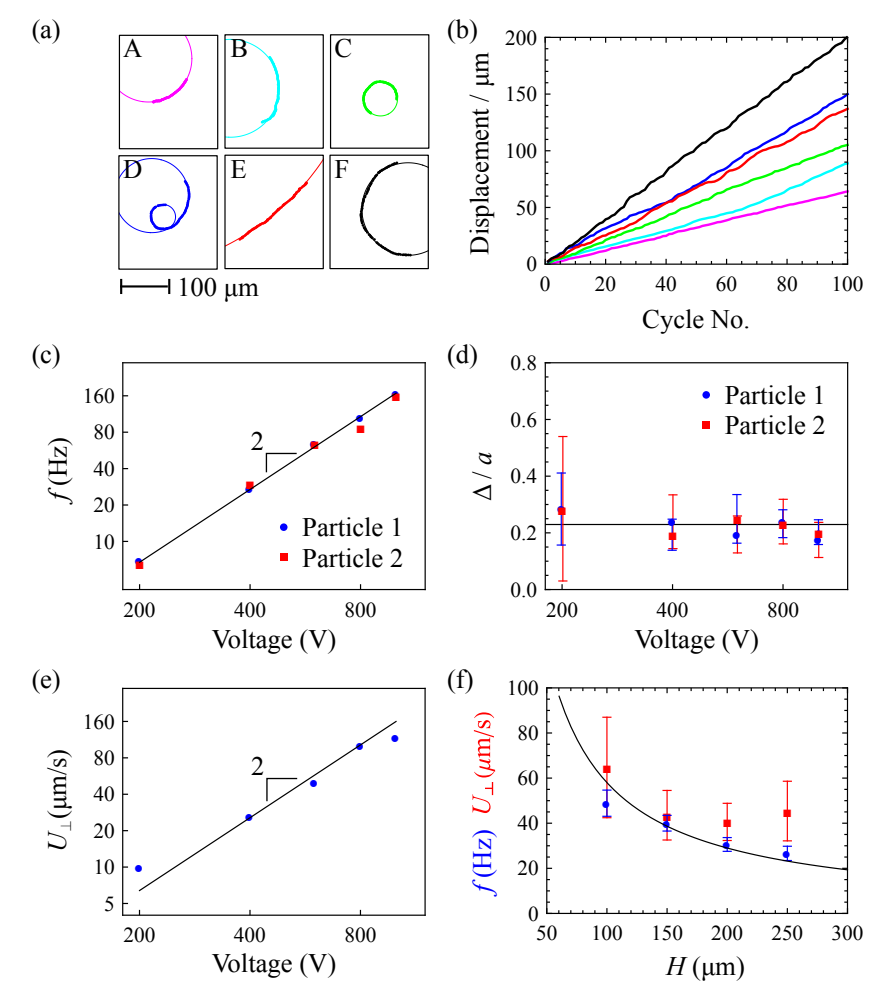


Figure 2: (a) Reconstructed particle trajectories of six Janus particles (radius  $a=4~\mu\mathrm{m}$ ; voltage  $V=800~\mathrm{V}$ ; electrode spacing  $H=200~\mu\mathrm{m}$ ). Markers denote the particle position at successive oscillations; curves are best circular fits to the data. (b) The cumulative displacement of particles in (a) increases linearly with the number of oscillation cycles. (c) The oscillation frequency of the particle scales quadratically with the voltage. Markers show data for two independent particles with an electrode spacing  $H=200~\mu\mathrm{m}$ ; the curve is a fit of the form  $f \propto V^2$ . (d) The lateral particle displacement  $\Delta$  during each oscillation is largely independent of the applied voltage. Markers show the mean displacement; error bars denote one standard deviation above and below the mean. (e) The particle velocity perpendicular to the field scales as the square of the voltage. Markers show data for one particle with an electrode spacing  $H=200~\mu\mathrm{m}$ ; the curve is a fit of the form  $U_{\perp} \propto V^2$ . (f) Particle frequency f and velocity  $U_{\perp}$  increase with decreasing electrode spacing H. Markers show the average of eight particles for a constant applied field  $V/H=4~\mathrm{V}/\mu\mathrm{m}$ ; error bars denote 95% confidence intervals. The curve is a fit of the form  $f \propto 1/H$ .

the charge on the particle changes sign thereby altering its preferred orientation in the field. The field-induced rotation of the particle in the vicinity of the electrode surface results in a lateral displacement, which is qualitatively similar to that of a sphere "rolling" along the surface. Successive rotations occur in a common direction towards the non-metallic hemisphere causing a steady lateral motion over the course of many oscillations. This putative mechanism is supported both by experimental observations of the transient particle orientation and by a mathematical model that describes the electrostatics and hydrodynamics of CCEP motion.

We used fluorescent particles to better visualize the orientation of Janus particles moving by CCEP. Such particles appeared bright when the metallic hemisphere was directed "down" (negative z-direction; away from the microscope objective) and dark when the metallic hemisphere was directed "up" (positive z-direction; towards the objective). For intermediate orientations, the fluorescent hemisphere of the particle was partially visible like the bright side of the moon in different phases. By focusing on planes in the middle of the two electrodes, we observed that particles moving downward appeared bright (gibbous moon) while those moving upward appeared dark (crescent moon) (Fig. 3b). By focusing on the lower electrode, we directly observed the rotation of the particle as it transitioned from the gibbous to crescent configuration (Fig. 3c). The opposite behavior was observed at the upper electrode where the particle rotated from the crescent to gibbous configuration (Fig. 3d). Importantly, the orientation of the Janus particle in the plane of the electrodes remained relatively constant from one cycle to the next, which allowed the particle to move steadily away from its metallic hemisphere.

To gain further insights into the propulsion mechanism, we use the equations of classical electrostatics and low-Reynolds number hydrodynamics to describe the dynamical trajectories of Janus particles moving by CCEP. We first consider the case of a single Janus particle with a net charge q in an unbounded medium subject to a uniform electric field  $\mathbf{E}$ . We solve for the electric potential within the dielectric and evaluate the electrostatic torque  $L(\alpha)$  on

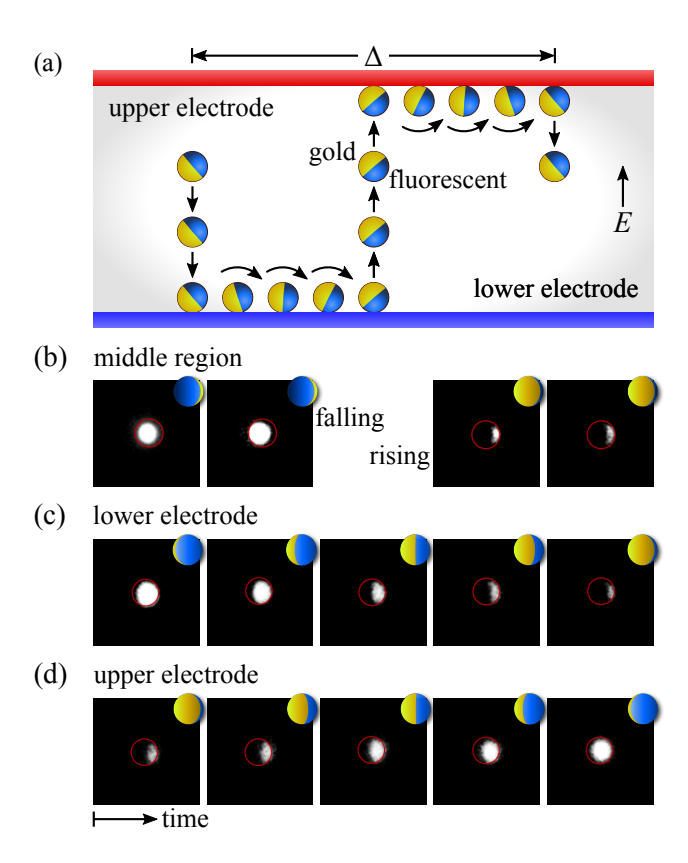


Figure 3: (a) Schematic illustration of the propulsion mechanism showing one oscillation cycle. Rotation of the particle near the electrodes results in a lateral displacement  $\Delta$ . (b-d) Fluorescent microscopy images highlight the non-metallic hemispheres of fluorescent Janus particles. Images are captured from above; the icons show the particles viewed from above using the color scheme from (a). Particles in the middle region (b) adopt a stable orientation that depends on their direction of travel (falling vs. rising). Upon contacting the lower (c) or upper (d) electrode, particles rotate in time from one orientation to another. See supporting video 4.

the particle as a function of its orientation  $\alpha$  relative to the field. For each charge, there exists one stable orientation for which the electric torque is zero  $L(\alpha) = 0$  and its derivative is negative  $L'(\alpha) < 0$  (Fig. 4a). Uncharged Janus particles tend to orient perpendicular to the applied field owing to the increased polarizability of their metallic hemisphere in that orientation ( $\alpha = \pi/2$  for q = 0). The addition of positive or negative charge, respectively, acts to rotate the particle towards or away from the direction of the field. When the charge exceeds a critical magnitude, the particle orients perfectly with or against the applied field. Importantly, this critical charge is similar in magnitude to that acquired by the particle during contact charging (see Fig. S4).

We now consider the dynamics of a particle "collision" with the lower electrode (Fig. 4b). Initially, the particle is positioned far from the electrode surface  $(z_p \gg a)$  with some fixed charge q. We solve for the electrostatic force and torque on the particle and compute the translational and rotational particle velocity in proximity to the surface. We then integrate these dynamical equations of motion to describe the position and orientation of a single particle as function of time. Figure 4b shows three different particle trajectories for different contact separations and a common charge  $q = 0.5q_s$  where  $q_s = 4\pi\varepsilon a^2 E$  is a convenient charge scale. The trajectories are in qualitative agreement with the experimental observations: a particle moves towards the electrode with a preferred orientation, reverses its charge on contact, rotates and translates as it adopts a newly preferred orientation, and ultimately moves away from the surface. The net lateral displacement  $\Delta$  depends on how closely the particle approaches the surface. For particles that approach more closely to the surface, their rotational motion is more tightly coupled to their lateral translation, and they move farther during each collision. The displacement also depends on the particle charge in an somewhat surprising way: highly charged particles  $(q > q_s)$  exhibit little or no displacement (Fig. S8). Such particles contact the surface with their axis aligned parallel with field and therefore experience little or no torque upon charge reversal. Instead, these particles move backward from the surface before ultimately rotating into the new stable orientation; particle rotation

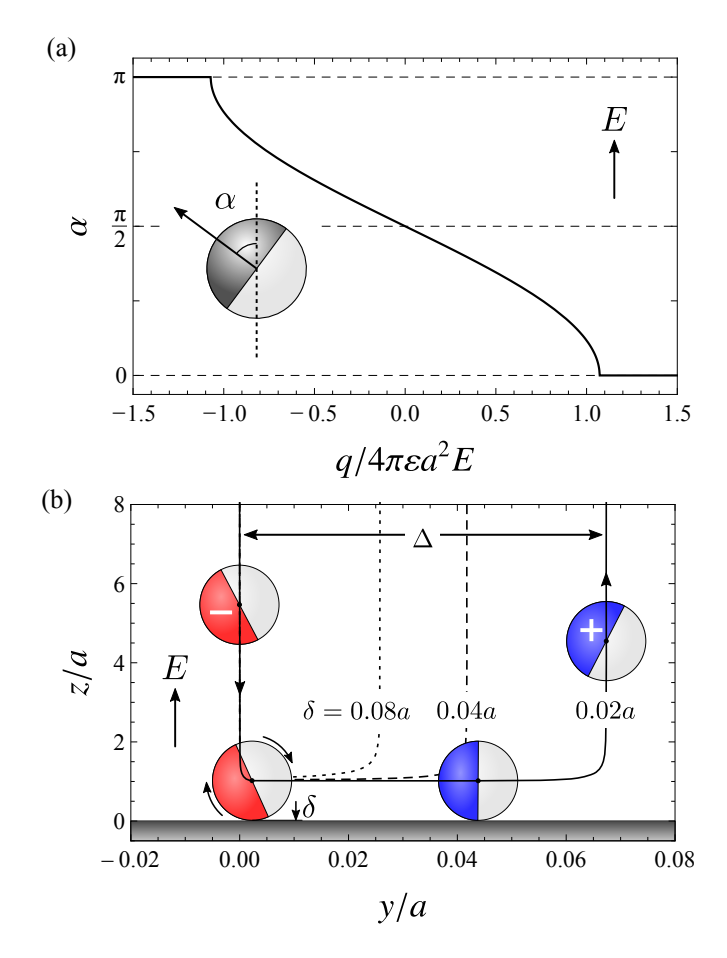


Figure 4: Results of the theoretical model. (a) The stable orientation  $\alpha$  of a Janus particle in a uniform electric field depends on the particle's charge q (scaled by  $q_s = 4\pi\varepsilon a^2 E$ ). Uncharged particles align perpendicular to the applied field E ( $\alpha = \pi/2$  for q = 0); highly charged particles align parallel to the field ( $\alpha = 0, \pi$  for  $|q| > 1.07q_s$ ). (b) Simulated particle "collisions" with the lower electrode for a particle charge  $q = \pm 0.5q_s$ . The solid curve shows the trajectory of the particle center; the orientation of the particle at different points along the trajectory is illustrated graphically. The net particle displacement  $\Delta$  depends on the surface separation  $\delta$  at contact when the particle charge reverses polarity. Note that for clarity the z and y axes use different scales.

far from the surface, however, results in little or no lateral displacement. This prediction of the model provides a plausible explanation for those particles that oscillate but do not translate perpendicular to the field.

There are some experimental observations that are not captured by the idealized model. Notably, the model predicts that particles should move along straight lines and not the circular trajectories observed in experiment. In the model, axial symmetry of the Janus particle allows for rotation about a single axis only – namely the x-axis in Fig. 4b; circular motions are therefore prohibited. Small deviations from axial symmetry, however, permit electric torques and rotations about the y-axis, which allow for the possibility of circular trajectories (torques or rotations about the z-axis are prohibited by symmetry of the applied field). The required particle asymmetries are small. Assuming that each oscillation cycle results in a translation  $\Delta = 0.2a$  and rotation  $\phi$ , the observed trajectories imply that  $\phi = \Delta/R \sim 0.01$  rad, where  $R \sim 10a$  is the radius of the circular trajectory.

The cause of these small deviations from axial particle symmetry are uncertain. Imperfections in the particles' metallic hemispheres are known to arise during metal deposition due to shadowing by neighboring particles.<sup>37</sup> Alternatively, the dielectric hemisphere may develop localized regions of electric charge on contact with the electrode surface. We confirmed experimentally that bare silica particles also charge and oscillate between the electrodes; however, the charging process is ca. 1000 times slower than for the conductive Janus particles (see Supporting Information for details). Either defect could potentially result in the type of electric torques necessary for achieving circular trajectories. Interestingly, in some experiments, the curvature of the particle trajectory changed abruptly during its motion (e.g., particle D in Fig. 2a). This observation may support a mechanism based on rare charging events on the dielectric hemisphere. Variability in the amount and distribution of charge on the dielectric surface may also explain the observed differences in speed among the different particles (Fig. 2; see Supporting Information for further discussion). Understanding these effects requires further study of non-axisymmetric particles of well defined shape and

surface charge distribution.

As noted above, the propulsion velocity is equal to the product of the oscillation frequency and the rotation-induced displacement:  $U_{\perp} = f\Delta$ . This expression suggests two basic strategies for maximizing the particle velocity: (i) increase the oscillation frequency,  $f \sim \varepsilon a V^2/\eta H^3$ , or (ii) increase the lateral displacement upon charge reversal. The oscillation frequency can be enhanced by increasing the voltage or by decreasing the spacing between the electrodes (Fig. 2e,f). Of course, the electrode spacing cannot be smaller than the particles themselves, and the electric field cannot exceed the dielectric strength of mineral oil (ca. 5 V/ $\mu$ m). To increase the rotation-induced displacement of the particle on charge reversal, it is necessary to alter the geometry of the particle itself (e.g., the size of the metallic patch). Such modifications can be challenging to achieve in practice and their consequences difficult to anticipate. Ultimately, the magnitude of the displacement is limited by the size of the particle ( $\Delta < a$ ).

Beyond the motions of individual particles, we observed several interesting behaviors in systems of two or more interacting particles (Fig. 5). When two particles were separated by a distance less than the electrode spacing (d < H), they influenced one another at a distance through electrostatic interactions. These interactions were either attractive or repulsive depending on the respective phases of the particle oscillations. Eike-charged particles oscillating "in phase" repelled one another as evidence by an increase in particle separation with time (Fig. 5a). By contrast, oppositely-charged particles oscillating "out of phase" moved toward one another in time (Fig. 5b). Due to slight differences in their oscillation frequencies, two particles often transitioned repeatedly between attractive and repulsive regimes. This particle "dance" could end in two different ways: either the particles moved off in different directions to find new partners, or they embraced one another to form a dynamic oscillating chain (a so-called bucket brigade  $^{49}$ ). Finally, we observed that interacting particles often moved together in a common direction – typically, along the line connecting the particle centers (Fig. 5c). Such coordinated motions were considerably faster than the

propulsion velocity of individual Janus particles perhaps suggesting an additional strategy for directing CCEP motions. Importantly, we confirmed that the above effects involving two or more particles were also observed among conductive, spherically isotropic (non-Janus) particles. Understanding the complex dynamics of multiple particles moving by CCEP will require further study beginning with the simplest spherical particles.

#### Conclusions

Contact charge electrophoresis drives the rapid oscillatory motion of conductive microparticles within nonpolar fluids. Particle asymmetries can be used to rectify such oscillatory motions to achieve directed transport perpendicular to the applied field. Rectified motions derive from particle rotations near the electrode surface upon contact charge transfer, which lead to repeated displacements in a common direction. This type of self-propulsion exhibits several characteristics that distinguish it from related systems based on self-phoresis, induced-charge electrophoresis, or Quicke rotation. Owing to the negligible electric currents through the nonpolar fluid, particle motions are highly efficient and require small energy inputs (ca. 1 nW / particle). 40 Rapid particle motions can enhance microscale mixing within nonpolar fluids, <sup>39</sup> which could be harnessed to accelerate catalytic reactions limited by mass transfer. Long-ranged electrostatic interactions among the particles results in complex collective motions relevant to the study of active matter. Importantly, the directed CCEP motions of asymmetric particles can in principle be engineered by tuning the particle shape and surface composition. The rational design of such active components is a critical prerequisite for constructing dynamic colloidal assemblies capable of useful functions – that is, colloidal machines.

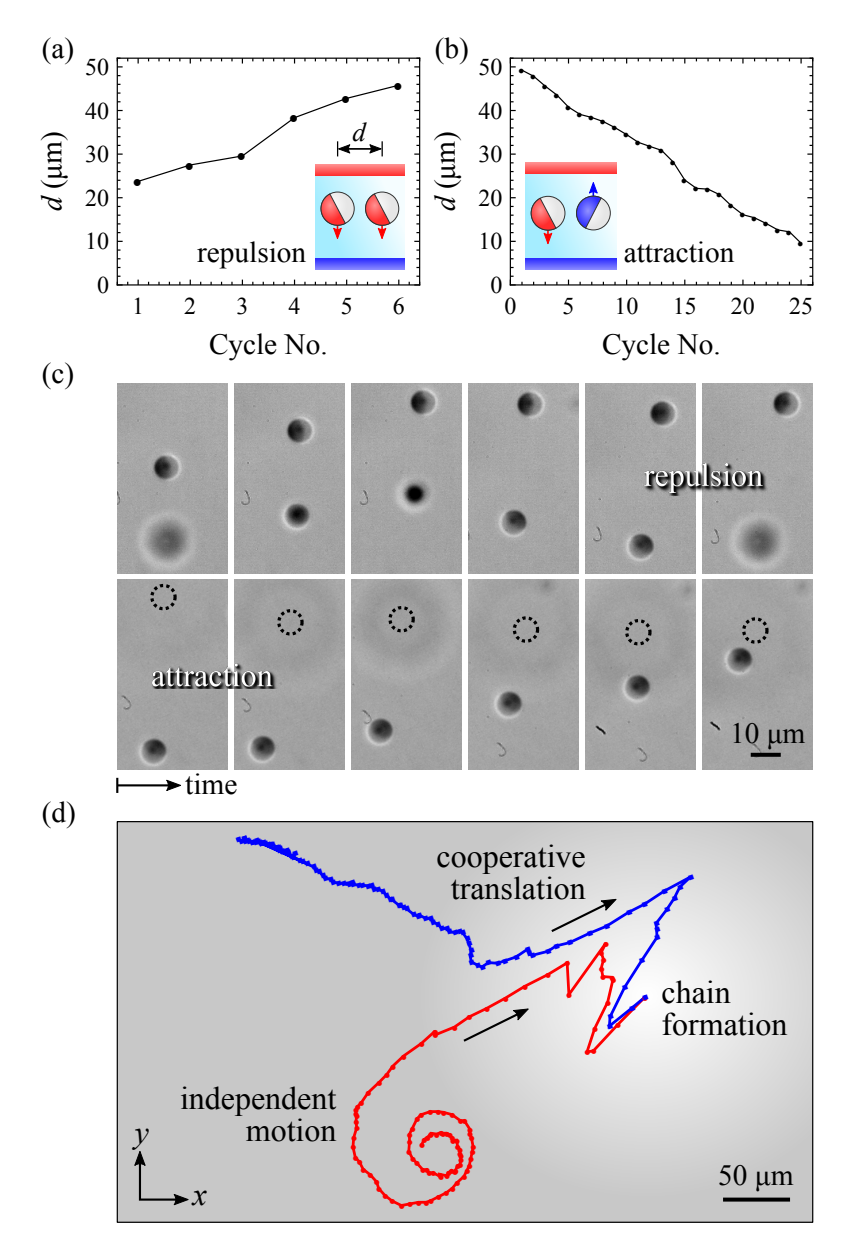


Figure 5: (a) The horizontal distance d between two particles oscillating in phase increases during each oscillation cycle. (b) The distance between particles moving out of phase decreases each cycle. (c) Image sequence corresponding to data shown in (a) and (b). (d) Reconstructed trajectories for two interacting particles. Initially, the particles are moving independently until their separation becomes less than the electrode spacing (here,  $H=150~\mu\mathrm{m}$ ). They then begin to move more quickly in a cooperative manner. Ultimately, the particles come together to form an oscillating chain. See supporting video 5.

#### **Associated Content**

#### **Supporting Information**

Description of supporting videos; Discussion of additional control experiments and estimates; Detailed description of the mathematical model. These materials are available free of charge via the Internet at http://pubs.acs.org.

#### **Author Information**

The authors declare no competing financial interest.

## Acknowledgement

This work was supported by the National Science Foundation under Grant No. CBET 1351704. SR and IK acknowledge partial funding from the National Science Foundation under Grant No. CBET 1264550.

## References

- (1) Ebbens, S. J. Active colloids: Progress and challenges towards realising autonomous applications. *Curr. Opin. Colloid Interface Sci.* **2015**, *21*, 14–23.
- (2) Li, J.; Rozen, I.; Wang, J. Rocket Science at the Nanoscale. *ACS Nano* **2016**, *10*, 5619–5634.
- (3) Dey, K. K.; Wong, F.; Altemose, A.; Sen, A. Catalytic MotorsQuo Vadimus? Curr. Opin. Colloid Interface Sci. 2016, 21, 4–13.
- (4) Lauga, E.; Powers, T. R. The hydrodynamics of swimming microorganisms. *Reports Prog. Phys.* **2009**, *72*, 096601.

- (5) Takagi, D.; Palacci, J.; Braunschweig, A. B.; Shelley, M. J.; Zhang, J. Hydrodynamic capture of microswimmers into sphere-bound orbits. *Soft Matter* **2014**, *10*, 1784–1789.
- (6) Das, S.; Garg, A.; Campbell, A. I.; Howse, J.; Sen, A.; Velegol, D.; Golestanian, R.; Ebbens, S. J. Boundaries can steer active Janus spheres. *Nat. Commun.* **2015**, *6*, 8999.
- (7) Gao, W.; Dong, R.; Thamphiwatana, S.; Li, J.; Gao, W.; Zhang, L.; Wang, J. Artificial micromotors in the mouse's stomach: A step toward in vivo use of synthetic motors. *ACS Nano* **2015**, *9*, 117–123.
- (8) Baylis, J. R.; Yeon, J. H.; Thomson, M. H.; Kazerooni, A.; Wang, X.; John, A. E. S.; Lim, E. B.; Chien, D.; Lee, A.; Zhang, J. Q.; Piret, J. M.; Machan, L. S.; Burke, T. F.; White, N. J.; Kastrup, C. J. Self-propelled particles that transport cargo through flowing blood and halt hemorrhage. Sci. Adv. 2015, 1, e1500379.
- (9) Soler, L.; Magdanz, V.; Fomin, V. M.; Sanchez, S.; Schmidt, O. G. Self-propelled micromotors for cleaning polluted water. *ACS Nano* **2013**, *7*, 9611–9620.
- (10) Li, J.; Singh, V. V.; Sattayasamitsathit, S.; Orozco, J.; Kaufmann, K.; Dong, R.; Gao, W.; Jurado-Sanchez, B.; Fedorak, Y.; Wang, J. Water-driven micromotors for rapid photocatalytic degradation of biological and chemical warfare agents. ACS Nano 2014, 8, 11118–11125.
- (11) Morales-Narváez, E.; Guix, M.; Medina-Sánchez, M.; Mayorga-Martinez, C. C.; Merkoçi, A. Micromotor enhanced microarray technology for protein detection. Small 2014, 10, 2542–2548.
- (12) Kagan, D.; Calvo-Marzal, P.; Balasubramanian, S.; Sattayasamitsathit, S.; Manesh, K. M.; Flechsig, G.-U.; Wang, J. Chemical sensing based on catalytic nanomotors: motion-based detection of trace silver. J. Am. Chem. Soc. 2009, 131, 12082–12083.

- (13) Wang, W.; Duan, W.; Ahmed, S.; Sen, A.; Mallouk, T. E. From one to many: Dynamic assembly and collective behavior of self-propelled colloidal motors. *Acc. Chem. Res.* **2015**, *48*, 1938–1946.
- (14) Ibele, M.; Mallouk, T. E.; Sen, A. Schooling behavior of light-powered autonomous micromotors in water. *Angew. Chem. Int. Ed.* **2009**, *48*, 3308–3312.
- (15) Nguyen, N. H. P.; Jankowski, E.; Glotzer, S. C. Thermal and athermal three-dimensional swarms of self-propelled particles. *Phys. Rev. E* **2012**, *86*, 011136.
- (16) Bricard, A.; Caussin, J.-B.; Desreumaux, N.; Dauchot, O.; Bartolo, D. Emergence of macroscopic directed motion in populations of motile colloids. *Nature* **2013**, *503*, 95–98.
- (17) Jie Zhang,; Jing Yan,; Steve Granick, Directed Self-Assembly Pathways of Active Colloidal Clusters. *Angew. Chem. Int. Ed.* **2016**, *55*, 5166–5169.
- (18) Palacci, J.; Sacanna, S.; Steinberg, A. P.; Pine, D. J.; Chaikin, P. M. Living crystals of light-activated colloidal surfers. *Science* **2013**, *339*, 936–940.
- (19) Marchetti, M. C.; Joanny, J. F.; Ramaswamy, S.; Liverpool, T. B.; Prost, J.; Rao, M.; Simha, R. A. Hydrodynamics of soft active matter. Rev. Mod. Phys. 2013, 85, 1143– 1189.
- (20) Golestanian, R.; Liverpool, T. B.; Ajdari, A. Designing phoretic micro- and nano-swimmers. New J. Phys. **2007**, 9, 126.
- (21) Brown, A.; Poon, W. Ionic effects in self-propelled Pt-coated Janus swimmers. *Soft Matter* **2014**, 4016–4027.
- (22) Howse, J. R.; Jones, R. A. L.; Ryan, A. J.; Gough, T.; Vafabakhsh, R.; Golestanian, R. Self-Motile Colloidal Particles: From Directed Propulsion to Random Walk. *Phys. Rev. Lett.* 2007, 99, 048102.

- (23) Jiang, H. R.; Yoshinaga, N.; Sano, M. Active motion of a Janus particle by self-thermophoresis in a defocused laser beam. *Phys. Rev. Lett.* **2010**, *105*, 268302.
- (24) Anderson, J. J. Colloid transport by interfacial forces. Annu. Rev. Fluid Mech. 1989, 21, 61–99.
- (25) Paxton, W. F.; Kistler, K. C.; Olmeda, C. C.; Sen, A.; St Angelo, S. K.; Cao, Y.; Mallouk, T. E.; Lammert, P. E.; Crespi, V. H. Catalytic nanomotors: autonomous movement of striped nanorods. J. Am. Chem. Soc. 2004, 126, 13424–13431.
- (26) Fournier-Bidoz, S.; Arsenault, A. C.; Manners, I.; Ozin, G. A. Synthetic self-propelled nanorotors. *Chem. Commun.* **2005**, 441–443.
- (27) Wang, Y.; Hernandez, R. M.; Bartlett, D. J.; Bingham, J. M.; Kline, T. R.; Sen, A.; Mallouk, T. E. Bipolar electrochemical mechanism for the propulsion of catalytic nanomotors in hydrogen peroxide solutions. *Langmuir* **2006**, *22*, 10451–10456.
- (28) Moran, J. L.; Wheat, P. M.; Posner, J. D. Locomotion of electrocatalytic nanomotors due to reaction induced charge autoelectrophoresis. *Phys. Rev. E* **2010**, *81*, 065302.
- (29) Squires, T. M.; Bazant, M. Z. Breaking symmetries in induced-charge electro-osmosis and electrophoresis. *J. Fluid Mech.* **2006**, *560*, 65–101.
- (30) Gangwal, S.; Cayre, O. J.; Bazant, M. Z.; Velev, O. D. Induced-charge electrophoresis of metallodielectric particles. *Phys. Rev. Lett.* **2008**, *100*, 058302.
- (31) Boymelgreen, A.; Yossifon, G.; Park, S.; Miloh, T. Spinning Janus doublets driven in uniform ac electric fields. *Phys. Rev. E* **2014**, *89*, 011003.
- (32) Dreyfus, R.; Baudry, J.; Roper, M. L.; Fermigier, M.; Stone, H. A.; Bibette, J. Microscopic artificial swimmers. *Nature* **2005**, *437*, 862–865.
- (33) Wang, W.; Castro, L. A.; Hoyos, M.; Mallouk, T. E. Autonomous motion of metallic microrods propelled by ultrasound. *ACS Nano* **2012**, *6*, 6122–6132.

- (34) Nadal, F.; Lauga, E. Asymmetric steady streaming as a mechanism for acoustic propulsion of rigid bodies. *Phys. Fluids* **2014**, *26*, 082001.
- (35) Ahmed, S.; Wang, W.; Gentekos, D. T.; Hoyos, M.; Mallouk, T. E. Density and Shape Effects in the Acoustic Propulsion of Bimetallic Nanorod Motors. *ACS Nano* **2016**, *10*, 4763–4769.
- (36) Perro, A.; Reculusa, S.; Ravaine, S.; Bourgeat-Lami, E. B.; Duguet, E. Design and synthesis of Janus micro- and nanoparticles. *J. Mater. Chem.* **2005**, *15*, 3745–3760.
- (37) Pawar, A. B.; Kretzschmar, I. Patchy particles by glancing angle deposition. *Langmuir* **2008**, *24*, 355–358.
- (38) Drews, A. M.; Lee, H.-Y.; Bishop, K. J. Ratcheted electrophoresis for rapid particle transport. *Lab Chip* **2013**, *13*, 4295–4298.
- (39) Cartier, C. A.; Drews, A. M.; Bishop, K. J. Microfluidic mixing of nonpolar liquids by contact charge electrophoresis. *Lab Chip* **2014**, *14*, 4230–4236.
- (40) Drews, A. M.; Cartier, C. A.; Bishop, K. J. Contact Charge Electrophoresis: Experiment and Theory. *Langmuir* **2015**, *31*, 3808–3814.
- (41) Um, T.; Hong, J.; Im, D. J.; Lee, S. J.; Kang, I. S. Electrically Controllable Microparticle Synthesis and Digital Microfluidic Manipulation by Electric-Field-Induced Droplet Dispensing into Immiscible Fluids. *Sci. Rep.* **2016**, *6*, 31901.
- (42) Spellings, M.; Engel, M.; Klotsa, D.; Sabrina, S.; Drews, A. M.; Nguyen, N. H.; Bishop, K. J.; Glotzer, S. C. Shape control and compartmentalization in active colloidal cells. *Proc. Natl. Acad. Sci. USA* 2015, 112, E4642–50.
- (43) Prevo, B. G.; Velev, O. D. Controlled, rapid deposition of structured coatings from micro-and nanoparticle suspensions. *Langmuir* **2004**, *20*, 2099–2107.

- (44) Sinn, I.; Kinnunen, P.; Pei, S. N.; Clarke, R.; McNaughton, B. H.; Kopelman, R. Magnetically uniform and tunable Janus particles. *Appl. Phys. Lett.* **2011**, *98*, 024101.
- (45) Blair, D.; Dufresne, E. The Matlab Particle Tracking Code Repository. http://physics.georgetown.edu/matlab/, Accessed: 2016-06-01.
- (46) Kim, S.; Karrila, S. J. Microhydrodynamics; Dover: New York, 2005; p 311.
- (47) Swan, J. W.; Brady, J. F. Simulation of hydrodynamically interacting particles near a no-slip boundary. *Phys. Fluids* **2007**, *19*, 113306.
- (48) Mersch, E.; Vandewalle, N. Antiphase synchronization of electrically shaken conducting beads. *Phys. Rev. E* **2011**, *84*, 061301.
- (49) Pelesko, J. A. A self-organizing bucket brigade. 2004 Int. Conf. Mems, Nano Smart Syst. Proc. Los Alamitos, 2004; pp 212–217.